A&A 588, A84 (2016)
DOI: 10.1051/0004-6361/201527201

Astronomy & Astrophysics

A reddening-free method to estimate the ^{56}Ni mass of Type Ia supernovae

S. Dhawan[1,2,3], B. Leibundgut[1,2], J. Spyromilio[1], and S. Blondin[4]

[1] European Southern Observatory, Karl-Schwarzschild-Strasse 2, 85748 Garching bei München, Germany
e-mail: sdhawan@eso.org
[2] Excellence Cluster Universe, Technische Universität München, Boltzmannstrasse 2, 85748 Garching, Germany
[3] Physik Department, Technische Universität München, James-Franck-Strasse 1, 85748 Garching bei München, Germany
[4] Aix Marseille Université, CNRS, LAM (Laboratoire d'Astrophysique de Marseille) UMR 7326, 13388 Marseille, France

Received 17 August 2015 / Accepted 29 December 2015

ABSTRACT

The increase in the number of Type Ia supernovae (SNe Ia) has demonstrated that the population shows greater diversity than has been assumed in the past. The reasons (e.g. parent population, explosion mechanism) for this diversity remain largely unknown. We investigated a sample of SNe Ia near-infrared light curves and correlated the phase of the second maximum with the bolometric peak luminosity. The peak bolometric luminosity is related to the time of the second maximum (relative to the B light curve maximum) as follows: $L_{\rm max}(10^{43}\ {\rm erg\ s^{-1}}) = (0.039 \pm 0.004) \times t_2(J)({\rm days}) + (0.013 \pm 0.106)$. ^{56}Ni masses can be derived from the peak luminosity based on Arnett's rule, which states that the luminosity at maximum is equal to the instantaneous energy generated by the nickel decay. We checked this assumption against recent radiative-transfer calculations of Chandrasekhar-mass delayed detonation models and find this assumption is valid to within 10% in recent radiative-transfer calculations of Chandrasekhar-mass delayed detonation models. The $L_{\rm max}$ vs. t_2 relation is applied to a sample of 40 additional SNe Ia with significant reddening ($E(B-V) > 0.1$ mag), and a reddening-free bolometric luminosity function of SNe Ia is established. The method is tested with the ^{56}Ni mass measurement from the direct observation of γ-rays in the heavily absorbed SN 2014J and found to be fully consistent. Super-Chandrasekhar-mass explosions, in particular SN 2007if, do not follow the relations between peak luminosity and second IR maximum. This may point to an additional energy source contributing at maximum light. The luminosity function of SNe Ia is constructed and is shown to be asymmetric with a tail of low-luminosity objects and a rather sharp high-luminosity cutoff, although it might be influenced by selection effects.

Key words. supernovae: general – supernovae: individual: 2014J – supernovae: individual: 2006X – supernovae: individual: 2007if

1. Introduction

Type Ia supernovae (SNe Ia) exhibit diverse observable properties. In addition to the spectral and colour differences, the peak luminosity of SNe Ia range over several factors (e.g. Suntzeff 1996, 2003; Li et al. 2011). The amount of ^{56}Ni, derived from the bolometric luminosity, (Contardo et al. 2000) and the total ejecta mass (Stritzinger et al. 2006a; Scalzo et al. 2014) also show a wide dispersion. The $M_{^{56}\rm Ni}$ distribution provides insight into the possible progenitor channels and explosion mechanisms for SNe Ia (see Hillebrandt & Niemeyer 2000; Livio 2000; Truran et al. 2012).

The uncertainty in the reddening correction directly affects the ability to derive accurate bolometric luminosities and ^{56}Ni masses derived from the peak luminosity. The total-to-selective absorption (R_V) appears systematically and significantly lower in the SN hosts than the canonical Milky Way R_V value of 3.1. Nobili & Goobar (2008) use a large sample of nearby SNe Ia to derive an average R_V that is significantly lower than 3.1. Taking spectroscopic features that correlate with luminosity into account, Chotard et al. (2011) found an R_V of 2.8 ± 0.3 that is consistent with the Milky Way value. However, objects with high extinction are seen to have an unusually low R_V (Phillips et al. 2013; Patat et al. 2015). Interstellar dust means that a correction for reddening in the Milky Way and the host galaxy needs to be applied. Our goal is to establish a relation between the bolometric peak luminosity and the ^{56}Ni mass that is independent of reddening.

The near infrared (NIR) light curve morphology of SNe Ia is markedly different from that in the optical. In particular, the light curves start to rebrighten about two weeks after the first maximum, resulting in a second peak. Recent studies (e.g. Biscardi et al. 2012; Dhawan et al. 2015) found that more luminous SNe Ia reach the second maximum in NIR filters at a later phase. This was predicted by Kasen (2006), who also indicated that the phase of the second maximum (designated in the following as t_2 and measured relative to the B-band light curve maximum) should be a function of the ^{56}Ni mass in the explosion. We expect that the phase of the second NIR maximum can be used to determine bolometric peak luminosity $L_{\rm max}$ and the amount of ^{56}Ni synthesized in the explosion.

In the following, we investigate the link between the peak bolometric luminosity ($L_{\rm max}$) and the phase of the second maximum in the NIR light curves (t_2). We use a sample of nearby SNe Ia with low host-galaxy extinction (described in Sect. 2) to determine $L_{\rm max}$ and then employ different methods to derive $M_{^{56}\rm Ni}$ (Sect. 3). This relation can then be used to derive $L_{\rm max}$ and $M_{^{56}\rm Ni}$ for all SNe Ia with a measured t_2, since the timing parameter is free of reddening corrections and allows us to include heavily reddened objects. We check our derivation against independent measurements of $M_{^{56}\rm Ni}$ with the nearby SN 2014J in

Table 1. Sample of SNe Ia with low reddening $E(B-V)_{\rm host} < 0.1$.

SN	μ	$E(B-V)_{\rm host}$	$E(B-V)_{MW}$	Reference	$t_2(Y)$ (d)	$t_2(J)$ (d)	$t_2(H)$ (d)	$L_{\rm max}$ (10^{43} erg/s)
SN2002dj	32.93 ± 0.30	0.096 ± 0.030	0.010 ± 0.003	P08	...	31.1 ± 1.8	23.0 ± 0.9	1.25 ± 0.26
SN2002fk	32.59 ± 0.15	0.009 ± 0.044	0.035 ± 0.003	C14	...	29.5 ± 0.2	25.8 ± 0.3	1.42 ± 0.23
SN2005M	35.01 ± 0.09	0.060 ± 0.021	0.027 ± 0.002	B14	28.9 ± 3.8	30.9 ± 0.7	...	1.19 ± 0.20
SN2005am	32.85 ± 0.20	0.053 ± 0.017	0.043 ± 0.002	B14	21.7 ± 0.1	21.3 ± 0.7	19.7 ± 0.7	1.10 ± 0.20
SN2005el	34.04 ± 0.14	0.015 ± 0.012	0.098 ± 0.001	B14	25.0 ± 0.1	24.6 ± 0.6	24.3 ± 0.7	1.01 ± 0.11
SN2005eq	35.46 ± 0.07	0.044 ± 0.024	0.063 ± 0.003	B14	37.5 ± 0.1	35.0 ± 0.7	25.1 ± 0.1	1.32 ± 0.20
SN2005hc	36.50 ± 0.05	0.049 ± 0.019	0.028 ± 0.001	B14	37.5 ± 0.1	36.5 ± 2.5	...	1.36 ± 0.30
SN2005iq	35.80 ± 0.15	0.040 ± 0.015	0.019 ± 0.001	B14	27.7 ± 0.1	24.2 ± 0.7	25.0 ± 0.1	1.07 ± 0.21
SN2005ki	34.73 ± 0.10	0.016 ± 0.013	0.027 ± 0.001	B14	26.8 ± 0.1	25.2 ± 1.7	20.5 ± 1.7	1.03 ± 0.27
SN2006bh	33.28 ± 0.20	0.037 ± 0.013	0.023 ± 0.001	B14	25.0 ± 0.3	22.9 ± 0.3	21.0 ± 0.6	0.86 ± 0.15
SN2007bd	35.73 ± 0.07	0.058 ± 0.022	0.029 ± 0.001	B14	28.3 ± 0.1	...	...	1.22 ± 0.13
SN2007on	31.45 ± 0.08	<0.007	0.010 ± 0.001	B14	18.7 ± 0.4	18.2 ± 0.1	14.1 ± 1.4	0.60 ± 0.09
SN2008R	33.73 ± 0.16	0.009 ± 0.013	0.062 ± 0.001	B14	15.5 ± 0.7	14.1 ± 0.7	...	0.53 ± 0.10
SN2008bc	34.16 ± 0.13	<0.019	0.225 ± 0.004	B14	32.9 ± 0.3	33.3 ± 0.2	31.0 ± 1.4	1.24 ± 0.19
SN2008gp	35.79 ± 0.06	0.098 ± 0.022	0.104 ± 0.005	B14	33.5 ± 1.2	35.7 ± 0.8	34.4 ± 0.7	1.29 ± 0.14
SN2008hv	33.84 ± 0.15	0.074 ± 0.023	0.028 ± 0.001	B14	25.0 ± 0.3	24.7 ± 0.3	21.9 ± 0.5	1.08 ± 0.16
SN2008ia	34.96 ± 0.09	0.066 ± 0.016	0.195 ± 0.005	B14	24.0 ± 0.7	25.6 ± 0.2	19.2 ± 0.9	1.13 ± 0.14
SN2011fe	28.91 ± 0.20	0.014 ± 0.010	0.021 ± 0.001	P13	...	30.0 ± 0.8	24.3 ± 0.6	1.10 ± 0.15

Notes. $E(B-V)$ references: P08: Pignata et al. (2008); C14: Cartier et al. (2014); B14: Burns et al. (2014); P13: Patat et al. (2013). The references for the SNe Ia are presented along with the extinction values and the distances employed for calculation of the (pseudo-) bolometric luminosity at maximum.

M 82 and SN 2006X (Sect. 4). With the reddening independent method, we can establish the luminosity function of SNe Ia at maximum and also derive the distribution of nickel masses among SN Ia explosions (Sect. 5). We finish by discussing the implications of this determination of the $M_{^{56}\rm Ni}$ distribution in the conclusions (Sect. 6).

2. Data

Our SN Ia sample is constrained to objects, which have NIR observations at late times ($t > 50$ days after B maximum) with well-sampled optical and NIR light curves to construct a (pseudo)bolometric light curve and measure t_2. The main source of NIR photometry of SNe Ia is the Carnegie Supernova Project (CSP; Contreras et al. 2010; Burns et al. 2011; Stritzinger et al. 2011; Phillips 2012; Burns et al. 2014). We add to this sample objects from the literature. We only included SNe Ia with observations near maximum from U to H filters. The full description of the selected SNe Ia can be found in Dhawan et al. (2015).

The sample of low-reddening SNe Ia is defined to circumvent the uncertainties of host galaxy extinction. The 18 objects are presented in Table 1. We use $E(B-V)_{\rm host}$ values from the literature. Only objects with $E(B-V)_{\rm host} < 0.1$ mag were included. Since we consider only objects that display the second maximum in their NIR light curves, this implies that most low-luminosity SNe Ia were excluded, especially SN 1991bg-like objects.

At maximum light the UV-optical-IR integrated luminosity represents >90% of the true bolometric luminosity (Blondin et al. 2015). We constructed *UBVRIJH* bolometric light curves for objects with sufficient photometry near maximum light in the optical and the NIR. The K filter data was excluded since only few SN Ia have well-sampled K light curves. We calculated the fraction of the flux emitted in K for a few well-observed SNe Ia with sufficient data and determined it to be around 1% to 3% of the UVOIR luminosity at maximum. Excluding the K-flux results in only a minor uncertainty in the final UVOIR luminosity.

Prior to deriving a bolometric flux for the low extinction sample (see Table 3), we applied a correction for the measured extinction following Cardelli et al. (1989). The assumed distances and their references can be found in Table 1.

3. Results

Based on our previous work (Dhawan et al. 2015), where we found strong correlations between various derived parameters of SNe Ia with t_2 in the Y and J filters, we argue that the bolometric maximum luminosity should also correlate with t_2. The sample of low-reddening SNe Ia described in Sect. 2 is used to establish the relation between t_2 and $L_{\rm max}$. The t_2 parameter has the advantage of being essentially independent of reddening and distance (relative to the calibration sample). With such a relation we will be in a position to derive the luminosity function of SNe Ia at maximum.

3.1. Correlation between $L_{\rm max}$ and t_2

Figure 1 displays a strong correlation between t_2 for the Y and J filter light curves and the bolometric (UVOIR) luminosity $L_{\rm max}$ (determined by fitting a spline interpolation to the UVOIR light curve) with Pearson coefficients $r = 0.88$ and $r = 0.86$, respectively, for the low-reddening sample. A much weaker trend is observed in the H filter light curve with $r \approx 0.60$.

The slope of the $L_{\rm max}$ vs. t_2 relation appears to flatten for objects with $t_2 \gtrsim 27$ d. This is most prominent in the Y band. However, we would require a larger sample to confirm this trend amongst the most luminous objects.

We fit a simple linear relation to the data

$$L_{\rm max} = a_i \cdot t_{2,i} + b_i, \quad (1)$$

which leads to the entries in Table 2 (for *YJH* filters). The corresponding fits are shown in Fig. 1. We compare our observed values to the $L_{\rm max}$ and t_2 from the DDC models of Blondin et al. (2013). Model spectra and light curves published in Blondin et al. (2013) based on delayed detonation explosions show similar correlations to those described herein.

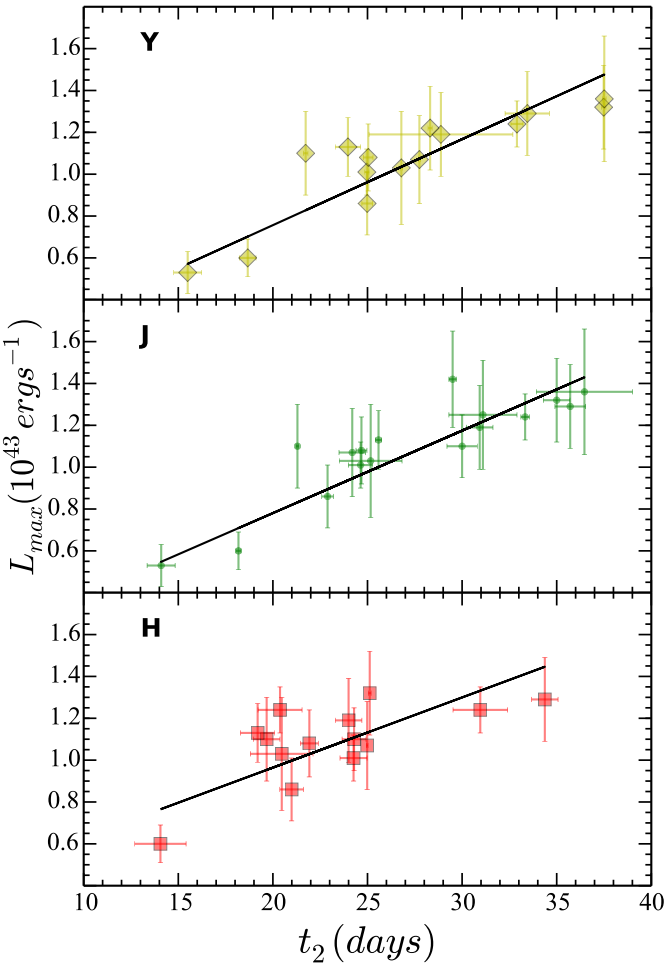

Fig. 1. Bolometric maximum luminosity $L_{\rm max}$ is plotted against the phase of the second maximum t_2 in YJH filter light curves. A strong correlation is observed in Y and J, whereas a weaker correlation is seen in the H band. Best fit lines are overplotted in black. The fit includes errors on both axes.

Table 2. Values of the coefficients for correlations between $L_{\rm max}$ and t_2 in the individual filters.

Filter	a_i	b_i
Y	0.041 ± 0.005	-0.065 ± 0.122
J	0.039 ± 0.004	0.013 ± 0.106
H	0.032 ± 0.008	0.282 ± 0.174

In the interest of a clean low extinction sample, we have removed seven objects with $E(B-V)_{\rm host} < 0.1$ but total $E(B-V) \geq 0.1$. Interestingly, several of the excluded objects are amongst the most luminous SNe Ia in the sample. Even after the removal of these seven objects, we do not derive a significant correlation for the H band light curves from our sample. It will have to be seen, whether future data will reveal a correlation or whether the H light curves are not as sensitive to the nickel mass as the other NIR filters. The relations are identical for the full and restricted sample within the uncertainties listed in Table 2. We combine the relations from the two bands for extrapolating the values of $L_{\rm max}$ in the following analysis. We assume that the Y band estimate is equivalent to the value in the J band and calculate the slope and intercept with the photometry of both filters, which leads to improved statistics.

3.2. Deriving $M_{^{56}\rm Ni}$ from $L_{\rm max}$

We present three different methods to derive $M_{^{56}\rm Ni}$ from $L_{\rm max}$: using Arnett's rule with an individual rise time for each SN Ia, using Arnett's rule with an assumed constant rise time applied to all SNe Ia, and calculating $L_{\rm max}$ from delayed detonation models with different $M_{^{56}\rm Ni}$ yields (Blondin et al. 2013). Arnett's rule states that at maximum light the bolometric luminosity equals the instantaneous rate of energy input from the radioactive decays. Any deviations from this assumption are encapsulated in a parameter α below. It is quite possible that α depends on the explosion mechanism and shows some variation between explosions (Branch 1992; Khokhlov et al. 1993). These early papers found rather wide ranges with $0.75 < \alpha < 1.4$ depending on the exact explosion model and the amount of assumed mixing (Branch 1992; Khokhlov et al. 1993). More recently Blondin et al. (2013) found a range of α within 10% of 1 for delayed detonation models. These models are not applicable for low-luminosity SNe Ia. If α systematically depends on explosion characteristics, then the derived nickel masses may suffer from a systematic drift not captured in our treatment. These uncertainties must be taken into account for interpreting the derived ^{56}Ni mass.

3.2.1. Arnett's rule with individual rise times

Arnett's rule states that the luminosity of the SN at peak is given by the instantaneous rate of energy deposition from radioactive decays inside the expanding ejecta (Arnett 1982; Arnett et al. 1985). This is summarized as (Stritzinger et al. 2006a):

$$L_{\rm max}(t_{\rm R}) = \alpha E_{^{56}\rm Ni}(t_{\rm R}), \tag{2}$$

where $E_{^{56}\rm Ni}$ is the rate of energy input from ^{56}Ni and ^{56}Co decays at maximum, $t_{\rm R}$ is the rise time to bolometric maximum, and α accounts for deviations from Arnett's Rule. The energy output from 1 $M_\odot$ of ^{56}Ni is ($\alpha = 1$):

$$\epsilon_{\rm Ni}(t_{\rm R}, 1\,M_\odot) = (6.45\times10^{43}e^{-t_{\rm R}/8.8} + 1.45\times10^{43}e^{-t_{\rm R}/111.3})\ {\rm erg\,s^{-1}}. \tag{3}$$

We use the relation for estimates with different rise times in the B filter for each SN following,

$$t_{{\rm R},B} = 17.5 - 5\cdot(\Delta m_{15} - 1.1) \tag{4}$$

from Scalzo et al. (2014), which covers the $t_{{\rm R},B}$–Δm_{15} parameter space of Ganeshalingam et al. (2011). Like Scalzo et al. (2014), we apply a conservative uncertainty estimate of ±2 days. The bolometric maximum occurs on average one day before $B_{\rm max}$ (Scalzo et al. 2014).

3.2.2. Arnett's rule with a fixed rise time

Originally, $M_{^{56}\rm Ni}$ was determined from $L_{\rm max}$ for a fixed rise time of 19 days for all SNe Ia (Stritzinger et al. 2006a). Similar to these analyses we propagate an uncertainty of ±3 days to account for the diversity in the rise times. The peak luminosity then becomes (Stritzinger et al. 2006a)

$$L_{\rm max} = (2.0 \pm 0.3)\times10^{43}(M_{^{56}\rm Ni}/M_\odot)\ {\rm erg\,s^{-1}}. \tag{5}$$

As described above, we assumed $\alpha = 1$ (see Stritzinger et al. 2006a; Mazzali et al. 2007), which is the analytical approximation of Arnett (1982). For the DDC models of Blondin et al. (2013), α is within 10% of 1 for all but the least luminous model.

Table 3. $M_{^{56}\mathrm{Ni}}$ measurements for low reddening SNe Ia.

SN	$M_{\mathrm{Ni}} - Arn$ ($M_\odot$)	err ($L_{\max}$) ($M_\odot$)	err (rise time) ($M_\odot$)	$M_{\mathrm{Ni}} - Arn$ (fixed rise) ($M_\odot$)	err ($L_{\max}$) ($M_\odot$)	err (rise time) ($M_\odot$)	$M_{\mathrm{Ni}} -$ DDC ($M_\odot$)
SN2002dj	0.59 ± 0.16	0.12	0.10	0.63 ± 0.16	0.13	0.10	0.61 ± 0.13
SN2002fk	0.68 ± 0.16	0.11	0.12	0.71 ± 0.17	0.12	0.12	0.76 ± 0.13
SN2005M	0.59 ± 0.14	0.10	0.10	0.60 ± 0.14	0.10	0.10	0.59 ± 0.11
SN2005am	0.47 ± 0.13	0.08	0.10	0.55 ± 0.14	0.10	0.10	0.52 ± 0.11
SN2005el	0.45 ± 0.10	0.05	0.09	0.51 ± 0.11	0.06	0.09	0.48 ± 0.07
SN2005eq	0.67 ± 0.15	0.10	0.11	0.66 ± 0.15	0.10	0.11	0.67 ± 0.11
SN2005hc	0.69 ± 0.19	0.15	0.12	0.68 ± 0.19	0.15	0.12	0.71 ± 0.16
SN2005iq	0.48 ± 0.13	0.09	0.09	0.54 ± 0.14	0.11	0.09	0.51 ± 0.10
SN2005ki	0.45 ± 0.14	0.11	0.09	0.51 ± 0.17	0.14	0.09	0.49 ± 0.14
SN2006bh	0.37 ± 0.10	0.06	0.08	0.43 ± 0.11	0.08	0.07	0.40 ± 0.07
SN2007bd	0.55 ± 0.13	0.06	0.11	0.61 ± 0.12	0.07	0.10	0.59 ± 0.10
SN2007on	0.23 ± 0.06	0.03	0.05	0.30 ± 0.07	0.05	0.05	0.28 ± 0.05
SN2008R	0.20 ± 0.06	0.04	0.05	0.27 ± 0.07	0.05	0.05	0.25 ± 0.06
SN2008bc	0.60 ± 0.14	0.09	0.11	0.62 ± 0.15	0.10	0.11	0.63 ± 0.11
SN2008gp	0.62 ± 0.13	0.06	0.11	0.65 ± 0.11	0.07	0.09	0.64 ± 0.09
SN2008hv	0.48 ± 0.11	0.07	0.09	0.54 ± 0.12	0.08	0.09	0.52 ± 0.09
SN2008ia	0.50 ± 0.12	0.06	0.10	0.57 ± 0.11	0.07	0.09	0.55 ± 0.09
SN2011fe	0.50 ± 0.12	0.07	0.10	0.55 ± 0.12	0.08	0.09	0.52 ± 0.10

Notes. The components of the error from $L_{\max}$ and rise time are given along with the total error.

3.2.3. Interpolating using delayed detonation models

We interpolate the relation between $L_{\max}$ (in a given filter set, u → H in this case) and $M_{^{56}\mathrm{Ni}}$ found from a grid of Chandrasekhar mass delayed detonation models of Blondin et al. (2013) to derive a ^{56}Ni mass from the observed peak luminosity for the sample presented in Table 1. The resulting ^{56}Ni mass estimates are presented in the bottom panel of Fig. 2. For all but the least luminous of these models, α is within 10% of 1 (Blondin et al. 2013).

3.3. Comparison of different methods

In Fig. 2, we plot the distributions of the $M_{^{56}\mathrm{Ni}}$, which were inferred for the low-reddening sample and which are from the different methods. Similar to previous studies we find that there is a large distribution in the $M_{^{56}\mathrm{Ni}}$ values for the sample in Table 1. We note over a factor of 2 difference between the lowest and highest $M_{^{56}\mathrm{Ni}}$ values (a factor of ∼3 for the variable rise time formalism). Unlike previous studies, this sample does not include faint, 91bg-like objects, since their NIR light curves do not display a second maximum. These objects are found to have a much lower $M_{^{56}\mathrm{Ni}} \sim 0.1\ M_\odot$ (Stritzinger et al. 2006a; Scalzo et al. 2014) from their peak luminosities. There is clearly a majority of objects with nickel masses between 0.4 and 0.7 $M_\odot$ with extensions to higher and lower masses. A further difference can be seen in Fig. 2 where the mass distribution between the case of individual and the fixed rise times is slightly different because observed rise times often are shorter than the assumed 19 days.

The individual errors clearly dominate the differences between the methods, and the results are not influenced by the chosen method. There appears a small systematic offset between the ^{56}Ni masses derived from DDC models and the ones with Arnett's rule and fixed rise time. The ^{56}Ni masses from the DDC models are about 0.05 $M_\odot$ lower, but well within the overall uncertainties, which are typically around 0.15 $M_\odot$ (Table 3).

For SN2011fe, Pereira et al. (2013) report a rise time of 16.58 days. Using this rise time, we obtain an $M_{^{56}\mathrm{Ni}}$ of 0.49 $M_\odot$ which is a 0.06 $M_\odot$ shift from the value using a 19 d rise. This shift is smaller than the uncertainty on the ^{56}Ni mass. For the low-reddening sample we note that the average difference between the fixed rise and variable rise formalisms is 0.04 $M_\odot$.

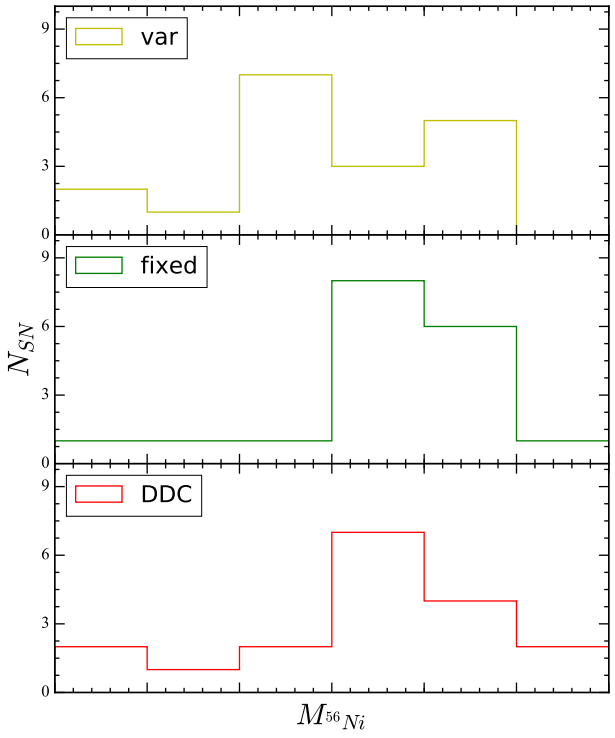

Fig. 2. Histograms of the different methods to estimate the $M_{^{56}\mathrm{Ni}}$ from the $L_{\max}$. The values found from Arnett's rule with fixed and individual rise times are plotted in the *top* and *middle* panels. The *bottom* panel displays the values estimated by using the relation between $L_{\max}$ and $M_{^{56}\mathrm{Ni}}$ found from the DDC models.

For the following analysis, we calculate the $M_{^{56}\mathrm{Ni}}$ using t_2. By substituting the relation derived between $L_{\max}$ and t_2 (Eqs. (1) and (3)), we obtain

$$\frac{M_{^{56}\mathrm{Ni}}}{M_\odot} = \frac{a_i \cdot t_2(i) + b_i}{\alpha \cdot \epsilon_{\mathrm{Ni}}(t_{\mathrm{R}}, M_\odot)}. \quad (6)$$

We mostly use the fixed rise time formalism in the following analysis, although in special cases, we also make use of the more accurately known rise time.

4. Test with well-observed SNe Ia

Dust in the host galaxy and the Milky Way makes determining the peak luminosity uncertain. Many nearby SNe Ia have shown marked deviations in the host galaxy dust properties from those observed in the Milky Way, mostly favouring a lower R_V value (Goobar 2008; Phillips et al. 2013). The extinction corrections are notoriously uncertain and directly affect our ability to measure peak bolometric luminosities of SNe Ia. Since t_2 is independent of reddening, we can use the derived correlation to determine the peak luminosity and estimate the ^{56}Ni mass for heavily reddened SNe Ia.

We tested this relation on SN 2014J, which has a direct γ-ray detection from the $^{56}\mathrm{Ni} \rightarrow {}^{56}\mathrm{Co}$ decay chain (Churazov et al. 2014; Diehl et al. 2015). Using the best fit relation for the reddening-free sample, we obtain $M_{^{56}\mathrm{Ni}} = 0.64 \pm 0.15\ M_\odot$ for a $t_2 = 31.99 \pm 1.15$ days and a rise time of 19 days. Since the error on the rise time is taken as ±3 days, we expect the error on $M_{^{56}\mathrm{Ni}}$ to decrease with a less conservative error estimate on t_R. Goobar et al. (2015) used Palomar Transient Factory (PTF) and Kilodegree Extremely Little Telescope (KELT) data to measure the rise time of SN 2014J. They find $t_\mathrm{R} = 17.25$ days. We placed a conservative error estimate of one day and evaluated the $M_{^{56}\mathrm{Ni}} = 0.60 \pm 0.10\ M_\odot$ which has a lower error bar than from the fixed rise time formalism.

The direct measurement of $M_{^{56}\mathrm{Ni}}$ for SN 2014J through the γ-ray detection gives an independent and fairly secure estimate of the nickel mass. Churazov et al. (2014) derive $^{56}\mathrm{Ni} = 0.62 \pm 0.13\ M_\odot$. Diehl et al. (2015) find a slightly lower mass of $M_{^{56}\mathrm{Ni}} = 0.56 \pm 0.10\ M_\odot$.

A detailed comparison of the derived ^{56}Ni masses is given in Table 4. The difficulty of the extinction correction and the advantage of the method presented here are obvious. The uncertainty in the γ-ray determination is due to the weakness of the signal and leads to slightly different interpretations. The very good correspondence between the direct $M_{^{56}\mathrm{Ni}}$ measurement and our relation of the second maximum in the NIR light curves is encouraging.

As a second case, we determine the bolometric peak luminosity L_max and the nickel mass $M_{^{56}\mathrm{Ni}}$ based on t_2 to the heavily extinguished SN 2006X. Wang et al. (2008) have derived a peak luminosity for this SN from multi-band photometry and a correction for dust absorption in the host galaxy. They determined a bolometric peak luminosity for SN 2006X of $(1.02 \pm 0.1) \times 10^{43}$ erg s^{-1}, which compares well with our measurement of $(1.14 \pm 0.16) \times 10^{43}$ erg s^{-1}. Wang et al. (2008) determined $M_{^{56}\mathrm{Ni}} = 0.50 \pm 0.05\ M_\odot$, which should be compared to $M_{^{56}\mathrm{Ni}} = 0.57 \pm 0.11\ M_\odot$ found from t_2 using the fixed rise time formalism. The measured rise time for SN 2006X is $t_\mathrm{R}(B) = 18.2 \pm 0.9$ d, which leads to $M_{^{56}\mathrm{Ni}} = 0.55 \pm 0.10\ M_\odot$. Table 5 presents several additional highly reddened SNe Ia, which had a previous determination of the nickel mass. The $M_{^{56}\mathrm{Ni}}$ for these objects were calculated in the same way as for SN 2014J and SN 2006X.

From Table 5, we can see that 1986G has a lower value of $M_{^{56}\mathrm{Ni}}$ than the other heavily reddened objects. This is consistent with the observed optical decline rate and lower B band luminosity (Phillips et al. 1987). Using nebular spectra, Ruiz-Lapuente & Lucy (1992) calculate the $M_{^{56}\mathrm{Ni}}$ for SN 1986G and find a value of $0.38 \pm 0.03\ M_\odot$. This is fully consistent with the estimate from t_2.

Scalzo et al. (2014) give $M_{^{56}\mathrm{Ni}}$ for SN 2005el and SN 2011fe. The comparison for SN 2011fe shows $M_{^{56}\mathrm{Ni}} = 0.52 \pm 0.15\ M_\odot$ from the NIR light curves, whereas Scalzo et al. (2014) find $M_{^{56}\mathrm{Ni}} = 0.42 \pm 0.08\ M_\odot$. The difference is mostly in the adopted value of α, 1.2 in Scalzo et al. (2014) compared to 1 in this study. Rescaling the value from Scalzo et al. (2014) to $\alpha = 1$, we obtain $M_{^{56}\mathrm{Ni}} = 0.50 \pm 0.08\ M_\odot$, which is fully consistent with our value. Pereira et al. (2013) report nickel masses for SN 2011fe for different values of α. Their nickel mass for $\alpha = 1$ is $M_{^{56}\mathrm{Ni}} = 0.53 \pm 0.11\ M_\odot$, nearly identical to our determination. For SN 2005el, Scalzo et al. (2014) obtain an $M_{^{56}\mathrm{Ni}}$ of $0.52 \pm 0.12\ M_\odot$. Scaled to an $\alpha = 1$, this gives $M_{^{56}\mathrm{Ni}} = 0.62$. We find $M_{^{56}\mathrm{Ni}} = 0.51 \pm 0.11\ M_\odot$, which is broadly consistent with the value found in Scalzo et al. (2014).

From the comparisons in Table 5, we conclude that there is good agreement between our values and those published in the literature. For SN 2001el we see that the error in the estimate from t_2 is substantially smaller than from the bolometric light curve.

One significant outlier is SN 2007if. This was presented as a super-Chandrasekhar-mass explosion (Scalzo et al. 2010) with a total luminosity of 3.2×10^{43} erg s^{-1}. The reddening from the host galaxy is somewhat unclear. There is no indication of Na foreground absorption, while the colour evolution and the Lira law would indicate some reddening. Any reddening would only increase the luminosity and the derived nickel mass based on Arnett's rule. The $M_{^{56}\mathrm{Ni}}$ estimate from t_2 for SN 2007if is significantly lower than the mass estimate through the bolometric peak luminosity by Scalzo et al. (2010). If we recalculate the $M_{^{56}\mathrm{Ni}}$ from the bolometric light curve presuming no extinction from the host galaxy, we obtain $M_{^{56}\mathrm{Ni}} = 1.6\ M_\odot$. This is a factor of ∼2 larger than our estimate. We discuss this supernova in Sect. 6.

5. The luminosity function of SNe Ia at maximum

We are now in a position to derive L_max for all SNe Ia with a reliably measured t_2 (as given in Tables 1 and 6) and establish the bolometric luminosity function of SNe Ia at maximum light. For objects in the low-reddening sample, we use the L_max determined from t_2 and the best-fit linear relation (green histogram in Fig. 3). Since the phase of the second maximum in the NIR is independent of the reddening, we can derive the reddening-free distribution of the luminosity function of SNe Ia (Fig. 3). We show here the histogram of 58 SNe Ia as derived from the Y and J light curves. The luminosity scale is based on the calibration sample of low-reddening objects (Sect. 3).

The luminosity function of SNe Ia is clearly not symmetric. The luminosity ranges slightly over a factor of 2. We find no obvious difference between the full sample and the low-reddening sample used to calibrate the relation between t_2 and L_max. If anything, the calibration sample has a flatter distribution with most SNe around 0.9×10^{43} erg s^{-1}, while the full sample includes more luminous objects. This could be an effect of the magnitude limit of the searches. The exact biases in our sample are difficult to define because it is not limited by volume.

The bolometric luminosity function can be compared to the R filter luminosity function derived by Li et al. (2011) based on 74 SNe Ia including the low-luminosity objects missing in our sample. The Li et al. (2011) magnitude-limited luminosity function (their Fig. 10) peaks at an absolute magnitude of ∼−19 with a few objects above −19.5 and a tail to fainter objects down

Table 4. Comparison of different methods of estimating $M_{^{56}\mathrm{Ni}}$ for SN 2014J.

M_{Ni} (inferred)	σ	Method	Reference
0.62	0.13	γ ray lines	Churazov et al. (2014)
0.56	0.10	γ ray lines	Diehl et al. (2015)
0.37	...	Bolometric light curve $A_V = 1.7$ mag	Churazov et al. (2014), Margutti et al. (2014)
0.77	...	Bolometric light curve $A_V = 2.5$ mag	Churazov et al. (2014), Goobar et al. (2014)
0.64	0.13	NIR second maximum	this work (combined fit)
0.60	0.10	NIR second maximum + measured rise	this work

Notes. All measurements assume a distance modulus of 27.64 ± 0.10.

Table 5. $M_{^{56}\mathrm{Ni}}$ estimates for objects with high values of $E(B-V)_{\mathrm{host}}$.

SN	t_2 (d)	$M_{^{56}\mathrm{Ni}}$ (inferred) ($M_\odot$)	$M_{^{56}\mathrm{Ni}}$ (lit. val.) ($M_\odot$)	Percent difference	Reference[a]
SN 1986G	16.4 ± 1.4	0.33 ± 0.08	0.38 ± 0.03	15.15	RL92
SN 1998bu	29.9 ± 0.4	0.58 ± 0.12	0.57	1.7	S06b
SN 1999ac	27.0 ± 2.0	0.53 ± 0.12	0.67 ± 0.29	26.4	S06a
SN 2001el	31.2 ± 0.7	0.62 ± 0.12	0.40 ± 0.38	33.8	S06a
SN 2002bo	28.9 ± 0.7	0.56 ± 0.12	0.52	7.1	St05
SN 2003cg	30.2 ± 1.5	0.59 ± 0.13	0.53	10.1	ER06
SN 2003hv	22.3 ± 0.1	0.43 ± 0.11	0.40 ± 0.11	6.9	L09
SN 2006X	28.2 ± 0.5	0.57 ± 0.11	0.50 ± 0.05	12.2	W08
SN 2007if	32.3 ± 0.8	0.65 ± 0.16	1.6 ± 0.1	158.3	S10

Notes. Comparison with independent estimates from the literature are given where available. [(a)] The references for the $M_{^{56}\mathrm{Ni}}$ measurements are RL92: Ruiz-Lapuente & Lucy (1992); S06a: Stritzinger et al. (2006a); S06b: Stritzinger et al. (2006b); St05: Stehle et al. (2005); ER06: Elias-Rosa et al. (2006); L09: Leloudas et al. (2009); W08: Wang et al. (2008); S10: Scalzo et al. (2010).

to −17. This is also reflected in our luminosity function (Fig. 3), where we observe a clear peak at $L_{\mathrm{max}} = 1.3 \times 10^{43}$ erg s^{-1} with some more luminous objects and a tail to fainter objects. The range is also comparable to the one found by Li et al. (2011).

In the next step we derive the distribution of $M_{^{56}\mathrm{Ni}}$ for all SNe Ia with sufficient infrared light curve data using Eq. (6) and a fixed rise time and $\alpha = 1$. Table 6 and Fig. 3 present the SN Ia nickel mass function.

6. Discussion and conclusion

Using the relation derived from the low-reddening sample, we extrapolate an L_{max} value for 58 SNe Ia objects having a measured t_2. The estimate of t_2, along with this relation, provides a method of deducing the bolometric peak luminosity, independent of a reddening estimate and of a distance measurement (relative to the calibration of our low-absorption sample) and without requiring multi-band photometry. We thus have established a reddening-free luminosity function of SNe Ia at peak (Fig. 3).

We established an intrinsic luminosity function and ^{56}Ni mass distribution for all SNe Ia with a t_2 measurement (Table 6). The distribution of L_{max} has a standard deviation of 0.2×10^{43} erg s^{-1}, and $M_{^{56}\mathrm{Ni}}$ has a standard deviation of 0.11 $M_\odot$. Scalzo et al. (2014) find a similar distribution of $M_{^{56}\mathrm{Ni}}$ with a σ of 0.16 $M_\odot$. We tested our method on SN 2014J, a heavily reddened SN Ia in the nearby galaxy M 82, and find good agreement between the estimates from the γ-ray observations (Churazov et al. 2014; Diehl et al. 2015, see Table 4). Faint, 91bg-like SNe Ia, which show typically lower luminosities (Filippenko et al. 1992; Leibundgut et al. 1993), do not display a second maximum in their NIR light curves and are not in our sample. Therefore, the true dispersion in peak luminosity and $M_{^{56}\mathrm{Ni}}$ for SN Ia will likely be larger than what is derived here. Stritzinger et al. (2006a) find a dispersion of a factor of ∼10, since their sample included peculiar SNe Ia, such as SN 1991bg and SN 1991T.

Our reddening-free estimate of the $M_{^{56}\mathrm{Ni}}$ can be compared to independent ^{56}Ni mass estimates, such as from the late-time (≥200 d) pseudo-bolometric light curve. It should also be possible to determine the amount of radiation emitted outside the UVOIR region of the spectrum at late phases and a bolometric correction (e.g. Leloudas et al. 2009). There are very few objects for which both NIR data to measure t_2 and nebular phase pseudo-bolometric observations are present, making a quantitative comparison for a sample of objects extremely difficult. Thus, we strongly encourage more late-time observations of SN Ia.

The observed L_{max} and $M_{^{56}\mathrm{Ni}}$ distributions directly connect to the physical origin of the diversity amongst SNe Ia. A possible explanation is the difference in the explosion mechanism. Pure detonations of M_{ch} WDs (Arnett 1969) were seen to be unfeasible since they burn the entire star to iron group elements and do not produce the intermediate mass elements (IMEs) observed in SN Ia spectra. Pure deflagrations (e.g. Travaglio et al. 2004) can reproduce observed properties of SNe with $M_{^{56}\mathrm{Ni}} \leq 0.4\,M_\odot$. Deflagration models however, cannot account for SNe with higher $M_{^{56}\mathrm{Ni}}$ and hence, cannot explain the entire distribution in Fig. 3.

Delayed-detonation models (e.g. Khokhlov 1991; Woosley 1990) are more successful at producing higher $M_{^{56}\mathrm{Ni}}$. In this explosion model, a subsonic deflagration expands the white dwarf to create low densities for IMEs to be produced in a supersonic detonation phase that is triggered at a deflagration-to-detonation transition density (ρ_{tr}).

Recent 1D studies by Blondin et al. (2013) compare a suite of Chandrasekhar mass (M_{Ch}) delayed detonation models with observations for SNe with a range of peak luminosities. They

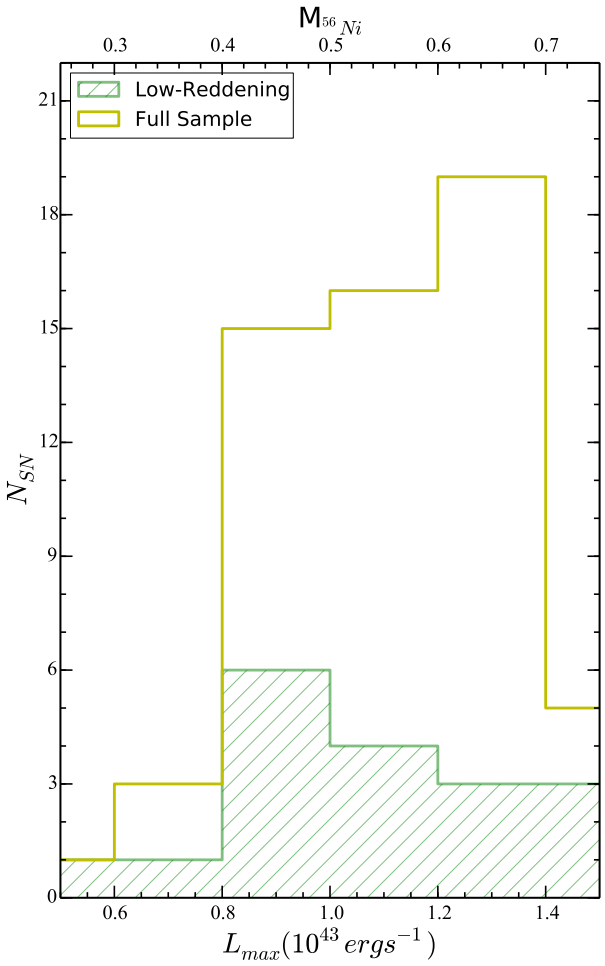

Fig. 3. Histogram distribution of $L_{\rm max}$ derived from the relations for the full sample of objects. Green: estimates of $L_{\rm max}$ for the low-reddening, calibration sample. Yellow: estimates for all objects with a t_2 measurement in the full sample. The axis labels on top correspond to the $M_{^{56}\rm Ni}$ estimate. We use the combined fit to obtain the final values.

.

find very good agreement of their models with photometric and spectroscopic observations at maximum. The range of $M_{^{56}\rm Ni}$ produced by their models corresponds well with the observations in Fig. 3, making these models strong candidates for explaining the observed diversity.

$M_{\rm Ch}$ explosion models can possibly account for the observed distribution in $M_{^{56}\rm Ni}$. Recent studies (e.g. van Kerkwijk et al. 2010), on the other hand, posit sub-Chandrasekhar mass explosions as a progenitor scenario for SNe Ia (e.g. see Woosley & Weaver 1994). This scenario is attractive since it can account for the progenitor statistics from population synthesis (see Livio 2000; Ruiter et al. 2013). Moreover, studies like Stritzinger et al. (2006a) and Scalzo et al. (2014) find a significant fraction of SNe Ia to have $M_{\rm ej} < 1.4\,M_{\odot}$, providing observational evidence for the sub-$M_{\rm Ch}$ progenitor scenario. We compare the luminosity function in Fig. 3 to the one obtained by Ruiter et al. (2013), using their violent merger models. They present a relation between primary white dwarf mass ($M_{\rm WD}$) and peak brightness for a grid of sub-$M_{\rm Ch}$ models. For objects in the lowest two bins of our luminosity distribution, the $M_{\rm WD}$ corresponds to 1 to 1.1 $_{\odot}$. For the highest luminosity objects, the models indicate an $M_{\rm WD}$ of 1.28 $M_{\odot}$. Thus, the luminosity function corresponds to a range

Table 6. $M_{^{56}\rm Ni}$ and $L_{\rm max}$ measurements for the complete sample of objects with t_2 measurements.

SN	$M_{^{56}\rm Ni}$ ($M_{\odot}$)	σ	$L_{\rm max}$ (10^{43} erg/s)	σ
1980N	0.42	0.10	0.84	0.21
1981B	0.63	0.13	1.26	0.21
1986G	0.33	0.07	0.66	0.18
1998bu	0.58	0.12	1.16	0.20
1999ac	0.53	0.12	1.05	0.20
1999ee	0.68	0.15	1.36	0.21
2000E	0.62	0.14	1.24	0.22
2000bh	0.65	0.14	1.30	0.22
2001bt	0.55	0.12	1.10	0.20
2001cn	0.58	0.13	1.19	0.20
2001cz	0.67	0.14	1.33	0.22
2001el	0.61	0.13	1.22	0.21
2002bo	0.56	0.11	1.12	0.21
2003cg	0.64	0.13	1.19	0.22
2003hv	0.43	0.10	0.84	0.17
2004ey	0.57	0.14	1.14	0.20
2004gs	0.43	0.11	0.85	0.18
2004gu	0.71	0.17	1.42	0.23
2005A	0.56	0.13	1.12	0.18
2005al	0.49	0.13	0.97	0.21
2005na	0.64	0.15	1.28	0.22
2006D	0.49	0.13	0.98	0.19
2006X	0.57	0.11	1.13	0.19
2006ax	0.62	0.15	1.24	0.21
2006et	0.64	0.16	1.27	0.22
2006gt	0.39	0.09	0.77	0.18
2006hb	0.41	0.11	0.81	0.19
2006kf	0.47	0.12	0.94	0.19
2007S	0.71	0.16	1.41	0.22
2007af	0.57	0.14	1.16	0.20
2007as	0.47	0.14	0.94	0.25
2007bc	0.55	0.14	1.09	0.20
2007bm	0.54	0.13	1.08	0.20
2007ca	0.66	0.16	1.29	0.22
2007if	0.65	0.16	1.30	0.22
2007jg	0.53	0.14	1.06	0.20
2007le	0.61	0.15	1.21	0.20
2007nq	0.46	0.13	0.92	0.20
2008C	0.63	0.16	1.26	0.23
2008fp	0.62	0.13	1.24	0.21
2014J	0.64	0.13	1.28	0.22

of sub-Chandrasekhar $M_{\rm WD}$, which provides further evidence of the plausibility of sub-$M_{\rm Ch}$ explosions as a progenitor scenario. The ^{56}Ni mass distribution (Fig. 3) is comparable to the yields from the models of Sim et al. (2010). Our $L_{\rm max}$ and $M_{^{56}\rm Ni}$ distributions do not allow us to distinguish which explosion mechanism is responsible for the observed variety.

We note that our sample includes one peculiar, super-$M_{\rm Ch}$ event, SN 2007if (Scalzo et al. 2010), with an estimated $M_{^{56}\rm Ni} = 0.65 \pm 0.16\ M_{\odot}$ using our technique. This is significantly lower than the value estimated in Scalzo et al. (2010) of $1.6 \pm 0.1\ M_{\odot}$. The t_2 estimate for this object is not exceptionally high, indicating a substantial but not exceptional amount of ^{56}Ni (similar to 91T-like SNe). One of the possible reasons for this discrepancy could be that the peak luminosity is not just a product of ^{56}Ni decay. This idea has been entertained in theoretical models for these super-$M_{\rm Ch}$ SN Ia. The models advocate a scenario of ejecta interaction with circumstellar material (CSM; see Hachinger et al. 2012; Dado & Dar 2015). There is also an indication of a shell interaction in this supernova (Scalzo et al. 2010),

and if this interaction results in increased peak luminosity, then the ^{56}Ni mass through Arnett's rule is overestimated. It could well be that additional energy is emitted in these super-$M_{\rm Ch}$ objects. A significant, but not extreme, amount of ^{56}Ni produced in the explosion along with interaction with the CSM could then explain the observed properties, such as lower ejecta velocities (~9000 km s^{-1}) and high peak luminosity. In Hachinger et al. (2012), the lower limit on $M_{^{56}\rm Ni}$ is ~0.6 $M_{\odot}$, which agrees well with our estimate.

The literature for such super-$M_{\rm Ch}$ objects with NIR light curves is still limited. Using the data in Taubenberger et al. (2011) for SN 2009dc, we obtained a t_2(J) of 31.7 ± 6.2 d, which corresponds to an $M_{^{56}\rm Ni}$ of 0.65 ± 0.18 $M_{\odot}$. Taubenberger et al. (2013) also argue for less extreme $M_{^{56}\rm Ni}$ based on late phase photometry and spectroscopy, although they prefer a comparatively higher $M_{^{56}\rm Ni}$ (~1 $M_{\odot}$) than our inferred value. One possible reason could be that the high ejecta densities lead to an earlier onset of the recombination wave than expected for normal Ia's, hence an earlier t_2 than is expected for a given ^{56}Ni mass. This would lead to an inference of lower $M_{^{56}\rm Ni}$ from t_2 for super-$M_{\rm Ch}$ SNe.

If we assume that the inferred ^{56}Ni mass from t_2 indicates the core ^{56}Ni for all SNe Ia the peak luminosity of super–$M_{\rm Ch}$ SNe Ia would be boosted by an additional energy source, such as shell interaction within the explosion. A good indicator could be the late bolometric decline phase and luminosity. This comparison would be much closer to the ^{56}Ni determination of the second peak than the peak bolometric luminosity.

Larger samples of well-observed SNe (e.g. Friedman et al. 2015) will help in improving the statistics of such a study. Future investigations with a detailed comparison between observations and a suite of sub-$M_{\rm Ch}$ detonation models will help shed more light on the nature of the progenitor scenario and explosion mechanism of SN Ia. Moreover, future theoretical studies of peculiar, super-$M_{\rm Ch}$ SNe will help in deciphering the nature of these extreme explosions.

Acknowledgements. This research was supported by the DFG Cluster of Excellence Origin and Structure of the Universe. B.L. acknowledges support for this work by the Deutsche Forschungsgemeinschaft through TRR33, The Dark Universe. We all are grateful to the ESO Visitor Programme for supporting the visit of S.B. to Garching. We would like to thank Rahman Amanullah for providing published photometry of SN2014J in the near infrared.

References

Arnett, W. D. 1969, Ap&SS, 5, 180
Arnett, W. D. 1982, ApJ, 253, 785
Arnett, W. D., Branch, D., & Wheeler, J. C. 1985, Nature, 314, 337
Biscardi, I., Brocato, E., Arkharov, A., et al. 2012, A&A, 537, A57
Blondin, S., Dessart, L., Hillier, D. J., & Khokhlov, A. M. 2013, MNRAS, 429, 2127
Blondin, S., Dessart, L., & Hillier, D. J. 2015, MNRAS, 448, 2766
Branch, D. 1992, ApJ, 392, 35
Burns, C. R., Stritzinger, M., Phillips, M. M., et al. 2011, AJ, 141, 19
Burns, C. R., Stritzinger, M., Phillips, M. M., et al. 2014, ApJ, 789, 32
Cardelli, J. A., Clayton, G. C., & Mathis, J. S. 1989, ApJ, 345, 245
Cartier, R., Hamuy, M., Pignata, G., et al. 2014, ApJ, 789, 89
Chotard, N., Gangler, E., Aldering, G., et al. 2011, A&A, 529, L4
Churazov, E., Sunyaev, R., Isern, J., et al. 2014, Nature, 512, 406
Contardo, G., Leibundgut, B., & Vacca, W. D. 2000, A&A, 359, 876
Contreras, C., Hamuy, M., Phillips, M. M, et al. 2010, AJ, 139, 519
Dado, S., & Dar, A. 2015, ApJ, 809, 32
Dhawan, S., Leibundgut, B., Spyromilio, J., & Maguire, K. 2015, MNRAS, 448, 1345
Diehl, R., Siegert, T., Hillebrandt, W., et al. 2015, A&A, 574, A72
Elias-Rosa, N., Benetti, S., Cappellaro, E., et al. 2006, MNRAS, 369, 1880
Filippenko, A. V., Richmond, M. W., Branch, D., et al. 1992, AJ, 104, 1543
Friedman, A. S., Wood-Vasey, W. M., Marion, G. H., et al. 2015, ApJS, 220, 9
Ganeshalingam, M., Li, W., & Filippenko, A. V. 2011, MNRAS, 416, 2607
Goobar, A. 2008, ApJ, 686, L103
Goobar, A., Kromer, M., Siverd, R., et al. 2014, ApJ, 784, L12
Goobar, A., Johansson, J., Amanullah, R., et al. 2015, ApJ, 799, 106
Hachinger, S., Mazzali, P. A., Taubenberger, S., et al. 2012, MNRAS, 427, 2057
Hillebrandt, W., & Niemeyer, J. C. 2000, ARA&A, 38, 191
Kasen, D. 2006, ApJ, 649, 939
Khokhlov, A. M. 1991, A&A, 245, 114
Khokhlov, A., Mueller, E., & Höflich, P. 1993, A&A, 270, 223
Leibundgut, B., Kirshner Robert, P., Phillips Mark, M., et al. 1993, AJ, 105, 301
Leloudas, G., Stritzinger, M. D., Sollerman, J., et al. 2009, A&A, 505, 265
Li, W., Bloom, J. S., Podsiadlowski, P., et al. 2011, MNRAS, 412, 1441
Livio, M. 2000, in Type Ia Supernovae, Theory and Cosmology, eds. J. C. Niemeyer, & J. W. Truran, Cambridge (Cambridge University Press), 33
Margutti, R., Parrent, J., Kamble, A., et al. 2014, ApJ, 790, 52
Mazzali, P. A., Röpke, F. K., Benetti, S., & Hillebrandt, W. 2007, Science, 315, 825
Nobili, S., & Goobar, A. 2008, A&A, 487, 19
Patat, F., Cordiner, M. A., Cox, N. L. J., et al. 2013, A&A, 549, A62
Patat, F., Taubenberger, S., Cox, N. L. J., et al. 2015, A&A, 577, A53
Pereira, R., Thomas, R. C., Aldering, G., et al. 2013, A&A, 554, A27
Phillips, M. M. 2012, PASA, 29, 434
Phillips, M. M., Phillips, A. C., Heathcote, S. R., et al. 1987, PASP, 99, 592
Phillips, M. M., Simon, J., D., Morrell, N., et al. 2013, ApJ, 779, 38
Pignata, G., Benetti, S., Mazzali, P. A., et al. 2008, MNRAS, 388, 971
Ruiter A. J., Sim, S. A., Pakmor, R., et al. 2013, MNRAS, 429, 1425
Ruiz-Lapuente, P., & Lucy, L. B. 1992, ApJ, 400, 127
Scalzo, R. A., Aldering, G., Antilogus, P., et al. 2010, ApJ, 713, 1073
Scalzo, R., Aldering, G., Antilogus, P., et al. 2014, MNRAS, 440, 1498
Sim, S. A., Röpke, F. K., Hillebrandt, W., et al. 2010, ApJ, 714, L52
Stehle, M., Mazzali, P. A., Benetti, S., & Hillebrandt, W. 2005, MNRAS, 360, 1231
Stritzinger, M., Leibundgut, B., Walch, S., & Contardo, G. 2006a, A&A, 450, 241
Stritzinger, M., Mazzali, P. A., Sollerman, J., & Benetti, S. 2006b, A&A, 460, 793
Stritzinger, M. D., Phillips, M. M., Boldt, L. N., et al. 2011, AJ, 142, 156
Suntzeff, N. B. 1996, in Supernovae and supernova remnants, eds. R. McCray, & Z. Wang (Cambridge: Cambridge University Press), 41
Suntzeff, N. B. 2003, in From Twilight to Highlight, The Physics of Supernovae, eds. W. Hillebrandt, & B. Leibundgut (Heidelberg: Springer), 183
Taubenberger, S., Benetti, S., Childress, M, et al. 2011, MNRAS, 412, 2735
Taubenberger, S., Kromer, M., Hachinger, S., et al. 2013, MNRAS, 432, 3117
Travaglio, C., Hillebrandt, W., Reinecke, M., & Thielemann, F.-K. 2004, A&A, 425, 1029
Truran, J. W., Glasner, A. S., & Kim, Y. 2012, J. Phys. Conf. Ser., 337, 012040
van Kerkwijk, M. H., Chang, P., & Justham, S. 2010, ApJ, 722, L157
Wang, X., Li, W., Filippenko, A. V., et al. 2008, ApJ, 675, 626
Woosley, S. E. 1990, BAAS, 22, 1221
Woosley, S. E., & Weaver, T. A. 1994, ApJ, 423, 371